Hydrol. Earth Syst. Sci., 21, 2015–2033, 2017
www.hydrol-earth-syst-sci.net/21/2015/2017/
doi:10.5194/hess-21-2015-2017

Hydrology and Earth System Sciences
Open Access
EGU

The effect of satellite-derived surface soil moisture and leaf area index land data assimilation on streamflow simulations over France

David Fairbairn, Alina Lavinia Barbu, Adrien Napoly, Clément Albergel, Jean-François Mahfouf, and Jean-Christophe Calvet

CNRM, UMR 3589 (Météo-France, CNRS), Toulouse, France

Correspondence to: Jean-Christophe Calvet (jean-christophe.calvet@meteo.fr)

Received: 26 April 2016 – Discussion started: 9 May 2016
Revised: 20 March 2017 – Accepted: 22 March 2017 – Published: 13 April 2017

Abstract. This study evaluates the impact of assimilating surface soil moisture (SSM) and leaf area index (LAI) observations into a land surface model using the SAFRAN–ISBA–MODCOU (SIM) hydrological suite. SIM consists of three stages: (1) an atmospheric reanalysis (SAFRAN) over France, which forces (2) the three-layer ISBA land surface model, which then provides drainage and runoff inputs to (3) the MODCOU hydro-geological model. The drainage and runoff outputs from ISBA are validated by comparing the simulated river discharge from MODCOU with over 500 river-gauge observations over France and with a subset of stations with low-anthropogenic influence, over several years. This study makes use of the A-gs version of ISBA that allows for physiological processes. The atmospheric forcing for the ISBA-A-gs model underestimates direct shortwave and long-wave radiation by approximately 5 % averaged over France. The ISBA-A-gs model also substantially underestimates the grassland LAI compared with satellite retrievals during winter dormancy. These differences result in an underestimation (overestimation) of evapotranspiration (drainage and runoff). The excess runoff flowing into the rivers and aquifers contributes to an overestimation of the SIM river discharge. Two experiments attempted to resolve these problems: (i) a correction of the minimum LAI model parameter for grasslands and (ii) a bias-correction of the model radiative forcing. Two data assimilation experiments were also performed, which are designed to correct random errors in the initial conditions: (iii) the assimilation of LAI observations and (iv) the assimilation of SSM and LAI observations. The data assimilation for (iii) and (iv) was done with a simplified extended Kalman filter (SEKF), which uses finite differences in the observation operator Jacobians to relate the observations to the model variables. Experiments (i) and (ii) improved the median SIM Nash scores by about 9 % and 18 % respectively. Experiment (iii) reduced the LAI phase errors in ISBA-A-gs but had little impact on the discharge Nash efficiency of SIM. In contrast, experiment (iv) resulted in spurious increases in drainage and runoff, which degraded the median discharge Nash efficiency by about 7 %. The poor performance of the SEKF originates from the observation operator Jacobians. These Jacobians are dampened when the soil is saturated and when the vegetation is dormant, which leads to positive biases in drainage and/or runoff and to insufficient corrections during winter, respectively. Possible ways to improve the model are discussed, including a new multi-layer diffusion model and a more realistic response of photosynthesis to temperature in mountainous regions. The data assimilation should be advanced by accounting for model and forcing uncertainties.

1 Introduction

Soil moisture influences the flow of water to rivers and aquifers on weekly to monthly timescales, which makes it an important factor in hydrological models. In the last two decades there have been considerable advances in soil moisture data assimilation (DA) using remotely sensed near-surface soil moisture (Houser et al., 1998; Crow and Wood, 2003; Reichle and Koster, 2005; Draper et al., 2012; de Rosnay et al., 2013). The estimation of global-scale soil moisture states has benefited considerably from a huge expansion of the satellite coverage, namely the Advanced Scatterom-

eter (ASCAT) instrument on board the METOP satellites (Wagner et al., 2007), the Soil Moisture and Ocean Salinity (SMOS) Mission (Kerr et al., 2001) and the Soil Moisture Active Passive (SMAP) Mission (Entekhabi et al., 2010), amongst others. However, these instruments can only indirectly observe the top 1–3 cm of soil moisture and the data are subject to retrieval errors. There are also spatial and temporal gaps in the observation coverage. The vegetation influences the soil moisture state through evapotranspiration and the vegetation coverage can be estimated by the leaf area index (LAI). This is a dimensionless quantity that represents the one-sided green leaf area per unit ground surface area (Gibelin et al., 2006). The LAI can be derived from satellite measurements in the visible range. However, over France it is available from polar-orbiting satellites at a relatively low temporal frequency (on average every 10 days) compared with soil moisture satellite observations (about every 3 days) due to cloud cover. The aim of DA methods is to combine these observations with a model forecast from the previous analysis (the background state) to provide an improved estimate of the state of the system (the analysis). DA methods are necessary to account for the errors in the observations and the model, and to spread the information through space and time.

Many studies have investigated the assimilation of surface soil moisture (SSM) and streamflow observations into hydrological models in order to improve streamflow predictions and hydrological parameters (Aubert et al., 2003; Moradkhani et al., 2005; Clark et al., 2008; Thirel et al., 2010; Moradkhani et al., 2012). For example, Thirel et al. (2010) used the best linear unbiased estimate (BLUE) method to assimilate streamflow observations into the MODCOU hydrogeological model over France, which they used to update soil moisture in the ISBA land surface model (LSM).

LSMs simulate water and energy fluxes between the soil and atmosphere. Unlike hydrological models, layer-based LSMs such as the ISBA model are typically point-wise (there is no horizontal interaction between the grid points), which greatly reduces the computational expense. A 1-D Kalman filtering approach (where observations are used to update collocated grid points only) is also implemented in this study, which is commonly applied to 1-D LSMs (Reichle et al., 2002; Draper et al., 2009; de Rosnay et al., 2013; Barbu et al., 2014).

In large-scale land surface DA, it is common to assimilate satellite-derived SSM observations and screen-level temperature and humidity observations into a LSM, in order to improve soil moisture and screen-level variables. Typically, the root-zone soil moisture (hereafter referred to as WG2) (1–3 m deep) is of more interest than SSM as it has a much larger water capacity and a long memory (from weeks to months). Land surface DA is often performed using an ensemble Kalman filter (EnKF) or a simplified extended Kalman filter (SEKF).

There has been increasing interest in ensemble DA for LSMs over the last two decades (Reichle et al., 2002, 2008; Zhou et al., 2006; Muñoz Sabater et al., 2007; Draper et al., 2012; Carrera et al., 2015), partly because these methods can estimate the "errors of the day" in the background-error covariance. The operational EnKF at Environment Canada is also motivated by coupling land surface DA with ensemble weather forecasting (Carrera et al., 2015). On the other hand, the SEKF simplifies the extended Kalman filter (EKF) by using fixed and uncorrelated background errors at the start of each cycle. Importantly, the SEKF generates flow-dependence and implicit background-error covariances from additional model integrations in the observation operator Jacobian calculations. Draper et al. (2009) found the flow-dependence from a 24 h assimilation window was sufficient to enable the SEKF to perform similarly to an EKF (which cycles the background-error covariance). Likewise, Muñoz Sabater et al. (2007) and Fairbairn et al. (2015) found that the SEKF and EnKF performed similarly, in spite of different linear assumptions.

Historically, the SEKF originated from a simplified 2D-Var (theoretically equivalent to an SEKF) scheme for the assimilation of screen-level temperature and humidity at the German Weather Service (DWD: Deutscher Wetterdienst) (Hess, 2001). An SEKF has been developed for research purposes to assimilate satellite-derived soil moisture at Météo-France (Mahfouf, 2010) and the UK Met Office (Candy et al., 2012), amongst other variables. The European Centre for Medium-Range Weather Forecast (ECMWF) model assimilates screen-level temperature and humidity operationally with an SEKF (de Rosnay et al., 2013) and since more recently has assimilated ASCAT-derived SSM observations (ECMWF, 2016).

In our study, we use an SEKF to assimilate LAI and SSM observations to update LAI and WG2 in the ISBA LSM within the SAFRAN–ISBA–MODCOU (SIM) hydrological suite. This study makes use of the A-gs version of ISBA that allows for physiological processes. SIM is operational at Météo-France and its streamflow and soil moisture outputs are used as a tool by the French National flood alert services (Thirel et al., 2010). SIM consists of three stages: (1) an atmospheric reanalysis (SAFRAN) over France, which forces (2) the ISBA-A-gs land surface model, which then provides drainage and runoff inputs to (3) the MODCOU distributed hydrogeological model. The drainage and runoff outputs from ISBA-A-gs are validated by comparing the simulated streamflow from MODCOU with observations. This study is relevant to the land surface DA community because several operational centres assimilate SSM observations using an SEKF to update WG2. Many studies have demonstrated that the force-restore dynamics of the ISBA three-layer model can effectively simulate soil moisture and propagate the increments downwards from the surface to the root zone (Muñoz Sabater et al., 2007; Draper et al., 2009; Mahfouf et al., 2009). An integrated validation using SIM

has demonstrated that the ISBA three-layer model can skilfully simulate drainage and runoff fluxes over France (Habets et al., 2008). The dynamic vegetation model in ISBA-A-gs is also capable of modelling seasonal changes in LAI (Jarlan et al., 2008; Brut et al., 2009; Barbu et al., 2011, 2014). But relatively few studies have assessed the SEKF performance using an integrated validation of the drainage and runoff fluxes. To our knowledge, this is the first article to consider this type of validation for LAI assimilation. Furthermore, the validation is robust because it is performed using more than 500 river gauges over France over several years.

This work is partly motivated by the study of Draper et al. (2011), who investigated the influence of assimilating ASCAT-derived SSM with an SEKF on SIM over France. They used a version of SIM with high-quality atmospheric forcing to represent the "truth" and lower-quality atmospheric forcing for the model. Although the SEKF seemed to improve the results in their study, they acknowledged that this may have been related to a bias in the SEKF rather than the assimilation accurately responding to the precipitation errors. Despite the fact that SAFRAN can be considered as a high-quality atmospheric forcing, studies by Szczypta et al. (2011) and Le Moigne (2002) have found underestimations of about 5 % in the direct shortwave and long-wave radiative fluxes respectively, averaged over France. In addition to these problems with radiative forcing, we demonstrate in this study that the LSM substantially underestimates LAI for grasslands in winter (compared with satellite retrievals). The specification of the LAI minimum in the model is important because it prevents vegetation mortality and allows the regrowth of vegetation in the spring period (Gibelin et al., 2006). We use SIM to validate the impact of four experiments on the drainage and runoff fluxes:

i. Correcting the model-underestimated LAI minimum parameter;

ii. Bias-correcting the SAFRAN radiative forcing;

iii. Assimilating only LAI observations with an SEKF;

iv. Assimilating SSM and LAI observations with an SEKF.

The first two experiments attempt to resolve systematic model issues, while experiments (iii) and (iv) assimilate data in order to correct random errors in the initial conditions.

Since Draper et al. (2011) already investigated the impact of assimilating SSM in ISBA on river discharges with MODCOU, it was not necessary to perform an experiment with the assimilation of SSM only. We validate the performance of these experiments using observations from more than 500 river gauges over France during the period July 2007 to August 2014. We include an additional validation using a subset of 67 stations with low-anthropogenic influence because the MODCOU hydrogeological model only accounts for natural features. It should be noted that a bias in the forecast model invalidates the assumption of bias-blind DA (Dee, 2005). We therefore repeat experiments (iii) and (iv) after applying (i) and (ii) in to explore whether the systematic model errors impact the SEKF performance.

The paper is structured as follows. The methods and materials are given in Sect. 2, which includes a description of the LSM, the assimilated observations, the DA methods, the experimental setup and the SIM validation. The results are presented in Sect. 3, including the impact of the model simulations and DA on the model state variables and the river discharge. A discussion in Sect. 4 considers potential solutions to the problems encountered in this study. Finally, the conclusions are given in Sect. 5.

2 Methods and materials

2.1 ISBA-A-gs land surface model

In our study, the ISBA-A-gs LSM was forced by the atmospheric variables provided by the "Système d'Analyse Fournissant des Renseignements à la Neige" (SAFRAN). The analyses of temperature, humidity, wind speed, and cloudiness are originally performed every 6 h using the ARPEGE (Action de Recherche Petite Echelle Grande Echelle) NWP (Numerical Weather Prediction) model (Courtier et al., 2001). The original precipitation analysis is performed daily at 06:00 UTC, to include in the analysis the numerous rain gauges that measure precipitation on a daily basis. A linear interpolation converts these values to the hourly SAFRAN forcing values (Quitana-Ségui et al., 2008). Instantaneous variables such as precipitation are assumed to be constant for each 15 min model time step during these hourly intervals, while other variables are linearly interpolated. The SAFRAN forcing is assumed to be homogeneous over 615 specified climate zones. The forcing is interpolated from these zones to a Lambert-projected grid with a horizontal resolution of 8 km (Durand et al., 1993). The delayed cut-off version of SAFRAN was employed, which uses information from an additional 3000 climatological observing stations (which report once a month) over France (Quitana-Ségui et al., 2008; Vidal et al., 2010) after the real-time cut-off, which makes the resulting analyses more accurate.

Version 8.0 of SURFEX was used in the experiments, which contains the "Interactions between Soil, Biosphere and Atmosphere" (ISBA) LSM (Noilhan and Mahfouf, 1996). The model uses the same horizontal grid resolution as SAFRAN of 8 km. The ISBA-A-gs version was used, which allows for the influence of physiological processes, including photosynthesis (Calvet et al., 1998). Each grid cell is split into twelve vegetation types (so-called "patches"). Soil and vegetation parameters are derived from the ECOCLIMAP database (Faroux et al., 2013). The nitrogen dilution version (referred to as "NIT" hereafter) of ISBA-A-gs was applied, which dynamically simulates the LAI evolution (Gibelin et al., 2006). The NIT version allows for the effects

of atmospheric conditions on the LAI, including the carbon dioxide concentrations.

The three-layer version of ISBA was adopted for this study (Boone et al., 1999). This includes the WG1 layer with depth 0–1 cm. The WG2 layer includes WG1 and is 1–3 m deep, with the depth depending on the patch type. A recharge zone exists below the WG2 layer. The model water transfers are governed by the force-restore method of Deardorff (1977). The surface and root-zone layers are forced by the atmospheric variables and restored towards an equilibrium value. The drainage and runoff outputs from ISBA-Ags drive the MODCOU hydrogeological model. The gravitational drainage is proportional to the water amount exceeding the field capacity (the effective limit where gravitational drainage ceases) (Mahfouf and Noilhan, 1996). It is driven by the hydraulic conductivity of the soil, which depends on its texture. A small residual drainage below field capacity was introduced by Habets et al. (2008) to account for unresolved aquifers. Runoff occurs when the soil moisture exceeds the saturation value.

2.2 Assimilated observations

The SSM observations were retrieved from ASCAT C-band spaceborne radar observations, which observe at 5.255 GHz and a resolution of approximately 25 km. The radar is onboard EUMETSAT's Meteorological Operational (MetOP) satellites. The assimilation of ASCAT data was chosen because it was available throughout the analysis period. The original backscatter values were converted into a surface degree of saturation (SDS, with values between 0 and 1) using a change detection technique, which was developed at the Vienna University of Technology and is detailed in Wagner et al. (1999) and Bartalis et al. (2007). The historically lowest and highest backscatter coefficient values are assigned to dry and saturated soils respectively. The Copernicus Global Land Service then calculates a soil wetness index (SWI) by applying a recursive exponential filter to these SDS values (Albergel et al., 2008) using a timescale that may vary between 1 and 100 days. The SWI represents the soil wetness over the soil profile and also has values between 0 (dry) and 1 (saturated). The longer the timescale of the exponential filter, the deeper the representative soil profile. The SWI-001 version 2.0 product was used in this study, which has a 1 day timescale and represents the SWI for a depth of up to 5 cm.

A surface-state flag is provided with the ASCAT product, which identifies frozen conditions, the presence of snow cover or temporary melting ice or water on the surface. Observations are screened during frozen surface conditions or when snow cover is present if the ASCAT flag is set to frozen. Additionally, observations with a topographic complexity flag greater than 15 % and/or a wetland fraction greater than 5 % (both provided with the ASCAT data) are removed. More information about ASCAT quality flags can be found in Scipal et al. (2005). After screening, the data were projected onto the 8 km resolution model grid by averaging all the data within 0.15° of each grid point (Barbu et al., 2014). As in Draper et al. (2011) an additional screening step was performed to remove observations whenever frozen conditions were detected in the model using a threshold temperature of 0° C. In addition, observations with an altitude greater than 1500 m and with an urban fraction greater than 15 % in the ECOCLIMAP database were removed.

In order to remove biases between model and observations, a linear rescaling to the SWI-001 data was conducted, which scales them such that the mean and standard deviations match the WG1 layer climatology (Calvet and Noilhan, 2000; Scipal et al., 2008). We found that it was necessary to rescale the SSM observations to match the SSM model climatology, partly because differences in the representation of the soil texture can cause very large systematic differences between the observations and the model. These differences are illustrated in terms of probability distribution in Fig. S4 of the Supplement. It shows the innovation histogram and the Gaussian fitting curve of the SSM product before rescaling.

This rescaling is a linear approximation of the cumulative distribution matching technique, which uses higher-order moments (Reichle et al., 2004; Drusch et al., 2005). As in Barbu et al. (2014), we applied a seasonal rescaling using a 3-month moving average over the experiment period (2007–2014). In the rescaling process the SWI-001 data are converted into the same units as the model, expressed in volumetric soil moisture ($m^3\,m^{-3}$). The rescaled SSM observations were assimilated into the WG1 model layer. The observations were assumed to occur at the same time as the analysis at 09:00 UTC and had a temporal frequency of about 3 days. This was a reasonable assumption since the satellite overpass is at 09:30 UTC and the atmospheric forcing is assumed to be constant over hourly intervals for instantaneous measurements such as precipitation. Therefore any discrepancies in SSM due to this 30 min time difference are small.

The GEOV1 LAI product is part of the European Copernicus Global Land Service. The LAI observations were retrieved from the SPOT-VGT (August 2007 to June 2014) and PROBA-V (June 2014 to July 2014) satellite data. The retrieval methodology is discussed by Baret et al. (2013). Following Barbu et al. (2014), the 1 km resolution observations were interpolated to the 8 km model grid points, provided that observations were present for at least 32 of the observation grid points (just over half the maximum amount). The observations were averaged over a 10-day period and assimilated at 09:00 UTC. This assumption was reasonable given that LAI evolves slowly. When considering removing systematic differences between the model and the observations, a linear rescaling of the LAI observations to the model climatology would be problematic because the model-observation bias is linked to model deficiencies. On the other hand, for SSM, systematic errors are related to the misspecification of physiographic parameters, such as the wilting point and the field capacity. As mentioned by several authors (e.g. Koster

et al., 2009; Albergel et al., 2012), the information content of soil moisture does not necessarily rely on its absolute magnitude but instead on its time variations. For SSM, the systematic bias between the model and the data consists mainly in their magnitude rather than their seasonal variability. Therefore this justifies the common approach used in land surface DA studies for the SSM variable. We should be aware that biases in soil moisture can show systematic variability, which may be due to model deficiencies rather that to the misspecification of certain parameters. It is not always possible to clearly determine which of the model features is to blame for the bias.

Contrary to SSM, the LAI bias between the model and the data has two components: one in magnitude and the other one in timing (see for example Fig. 6 in Barbu et al., 2014). When compared with the satellite data, the LAI model dynamics clearly show a shift in the seasonal cycle, mainly caused by model errors. The remote sensing LAI measurements potentially encapsulate realistic environmental features that are not represented or are incorrectly represented by the model. Forcing the data to conform to the model climatology would result in a loss of relevant information. Therefore, in this context, a rescaling of the LAI data to the model climatology was not considered. Furthermore, Barbu et al. (2014) found that the assimilation without rescaling can cope with these model errors.

2.3 Data assimilation

The SEKF simplifies the EKF (Jazwinski, 1970) by using a fixed estimate of the background-error variances and zero covariances at the start of each cycle (Mahfouf et al., 2009). Implicit background-error covariances between the layers and the prognostic variables are generated at the analysis time by the model integration in the observation operator Jacobians. We used the same SEKF formulation as Barbu et al. (2014) for the assimilation of SSM and LAI observations over France. The prognostic variables are LAI and WG2. The WG1 layer is not included in the analysis update because it is a shallow layer (1 cm depth) that is driven by the atmospheric forcing rather than the initial conditions (Draper et al., 2009; Barbu et al., 2014). The background state ($\boldsymbol{x}^{\mathrm{b}}$) at time t_i is a model propagation of the previous analysis ($\boldsymbol{x}^{a}(t_{i-1})$) to the end of the 24 h assimilation window:

$$\boldsymbol{x}^{\mathrm{b}}(t_i) = M_{i-1}(\boldsymbol{x}^{\mathrm{a}}(t_{i-1})), \tag{1}$$

where M is the (nonlinear) ISBA-A-gs model. The observation was assimilated at the analysis time (09:00 UTC), at the end of the 24 h assimilation window. The analysis was calculated from the generic Kalman filter equation:

$$\boldsymbol{x}^{\mathrm{a}}(t_i) = \boldsymbol{x}^{\mathrm{b}}(t_i) + \mathbf{K}_i(\boldsymbol{y}_i^{\mathrm{o}} - \boldsymbol{y}_i), \tag{2}$$

where $\boldsymbol{y}^{\mathrm{o}}$ is the assimilated observation and $\boldsymbol{y}_i = H(\boldsymbol{x}^{\mathrm{b}}(t_i))$ is the model-predicted value of the observation at the analysis time. The Kalman gain is defined as follows:

$$\mathbf{K}_i = \mathbf{B}_i\mathbf{H}_i^{\mathrm{T}}(\mathbf{H}_i\mathbf{B}_i\mathbf{H}_i^{\mathrm{T}} + \mathbf{R}_i)^{-1}, \tag{3}$$

where $\mathbf{H}$ is the Jacobian matrix of the linearized observation operator, $\mathbf{B}$ is the background-error covariance matrix and $\mathbf{R}$ is the observation-error covariance matrix. The observation operator Jacobians were calculated using finite differences for observation k and model variable l:

$$\mathbf{H}_i^{kl} = \frac{H_i^k(M_{i-1}(\boldsymbol{x}(t_{i-1}) + \Delta x_{i-1}^l)) - H_i^k(M_{i-1}(\boldsymbol{x}(t_{i-1})))}{\Delta x_{i-1}^l}, \tag{4}$$

where Δx^l is a model perturbation applied to model variable l. The WG2 and LAI perturbations were set to $1.0\times10^{-4}\times(w_{\mathrm{fc}} - w_{\mathrm{wilt}})$ and $1.0\times10^{-3}\times$ LAI respectively. These were within the range of acceptable perturbation sizes based on the experiments of Draper et al. (2009) and Rüdiger et al. (2010). Equation (4) requires a 24 h model simulation for each prognostic variable, which implicitly propagates the background-error covariance from the start of the window to the time of the observations at the end of the window. The linear assumptions in deriving the Jacobians are generally acceptable for these perturbation sizes. However, occasionally the linear assumptions can break down, especially during dry periods in summer (Draper et al., 2009; Fairbairn et al., 2015). For this reason we set an upper bound on the soil moisture Jacobians of 1.0. It is worth mentioning that in situations where the model and atmospheric forcing errors are not properly taken into account, the SEKF analysis will be suboptimal even if the Jacobians are accurately computed. The Jacobian matrix derived from Eq. (4) is defined as follows:

$$\mathbf{H} = \begin{pmatrix} \frac{\partial \mathrm{WG1}}{\partial \mathrm{WG2}} & \frac{\partial \mathrm{WG1}}{\partial \mathrm{LAI}} \\ \frac{\partial \mathrm{LAI}}{\partial \mathrm{WG2}} & \frac{\partial \mathrm{LAI}}{\partial \mathrm{LAI}} \end{pmatrix}. \tag{5}$$

When assimilating just LAI, only the $\frac{\partial \mathrm{LAI}}{\partial \mathrm{WG2}}$ and $\frac{\partial \mathrm{LAI}}{\partial \mathrm{LAI}}$ terms are included. The $\frac{\partial \mathrm{WG1}}{\partial \mathrm{LAI}}$ is generally small, since the LAI does not substantially influence the surface layer (Barbu et al., 2014). The $\frac{\partial \mathrm{WG1}}{\partial \mathrm{WG2}}$ Jacobian couples WG1 with WG2 (Draper et al., 2009). The $\frac{\partial \mathrm{LAI}}{\partial \mathrm{WG2}}$ couples LAI with WG2 (Barbu et al., 2014). The $\frac{\partial \mathrm{LAI}}{\partial \mathrm{LAI}}$ Jacobian was studied by Rüdiger et al. (2010) and has a strong seasonal dependence. As we will demonstrate in Sect. 3.3, the examination of these Jacobians is essential in order to understand the performance of the SEKF.

SURFEX is implemented using the mosaic approach of Koster and Suarez (1992), where each model grid box is split into 12 vegetation patches. The SEKF analysis is calculated independently for each patch using the Jacobians for each individual patch but with one mean observation per grid box. The analysis for the grid point is calculated by aggregating the analyses over the 12 patches, which are weighted according to their patch fractions (see Barbu et al., 2014, for further

details). Taking into account the grid heterogeneity has been the justification for including vegetation patches in the model and in the assimilation scheme. The assimilation scheme uses the hypothesis that the distribution of innovations is proportional to the cover area. The analysis is adapted to plant functional types via the patch fractions and via the Jacobians.

Following Draper et al. (2011), the WG2 background-error standard deviation was set to $0.2(w_{fc} - w_{wilt})$, where w_{fc} is the field capacity and w_{wilt} is the wilting point. The scaling by $(w_{fc} - w_{wilt})$ assumes that there is a linear relationship between the soil moisture errors and the dynamic range, which depends on soil texture (Mahfouf et al., 2009). The SSM observation error standard deviation was set to $0.65(w_{fc} - w_{wilt})$, which is about $0.055\,m^3\,m^{-3}$ averaged over France. This value is slightly larger than the median ASCAT-derived SDS error of $0.05\,m^3\,m^{-3}$ estimated by Draper et al. (2011) because it also approximates the oversampling issue i.e. the same ASCAT observation covers several grid points. This reduces the size of the analysis increments by approximately 10 %. This value is comparable with observation errors expected for remotely sensed SSM observations (de Jeu et al., 2008; Draper et al., 2013). As in Barbu et al. (2011), the LAI background and observation error standard deviations were proportional to the LAI values themselves and a value of $0.2 \times$ LAI was used for LAI values greater than $2\,m^2\,m^{-2}$. For LAI values below $2\,m^2\,m^{-2}$ the LAI errors were fixed at $0.4\,m^2\,m^{-2}$. Both the background-error and observation-error covariance matrices of the SEKF are diagonal (zero covariances between layers), but implicit background-error covariances are derived from the **H** matrix at the analysis time. The SEKF is a point-wise method, i.e. it cannot take into account horizontal covariances between grid points.

2.4 Experimental setup

The main experiments in this study are summarized in Table 1. The SIM river discharge was compared with the observations from 546 stations over France. Firstly the baseline experiment (NIT) was performed, which shows the impact of the biased radiative forcing and the underestimated LAI minimum on the SIM river discharge. Thereafter, two potential solutions to these deficiencies were investigated, as set out in the introduction: (i) NIT_m, which was equivalent to NIT but with an elevated LAI minimum of $1.2\,m^2\,m^{-2}$ for grasslands (as opposed to $0.3\,m^2\,m^{-2}$ with NIT), and (ii) NIT_{bc}, which used both the elevated LAI minimum of $1.2\,m^2\,m^{-2}$ and the bias-corrected radiative forcing (+5 % for direct long-wave and shortwave over France). Two DA experiments were undertaken to correct random errors in the initial conditions: (iii) LDAS1, which used the SEKF to assimilate only LAI with the NIT model, and (iv) LDAS2, which assimilated both LAI and SSM observations with the NIT model. The LAI minimum parameter is required to calculate a minimum level of photosynthesis at the start of the growing season. The default model value is arbitrarily fixed at $0.3\,m^2\,m^{-2}$ for grasslands, which is low enough to account for possible fluctuations in the LAI minimum due to climatic and interannual variability over France (Gibelin et al., 2006). However, we found that over 99 % of points with a high percentage of grassland (the grassland patch fraction exceeding 70 %) had an observed average annual LAI minimum above $1.2\,m^2\,m^{-2}$ during the experiment period (2007–2014). But the modelled LAI is frequently kept at the prescribed LAI minimum parameter during winter dormancy and is therefore systematically underestimated over most grassland regions in winter when compared to the satellite-derived observations. Similar issues were found by Brut et al. (2009), Lafont et al. (2012) and Barbu et al. (2014) when comparing the model with both MODIS and SPOT-VGT satellite-derived observations. Systematic differences between the model and the observations can be removed by calibrating model parameters (Kumar et al., 2012), which was the motivation for increasing the grassland LAI minimum parameter from 0.3 to $1.2\,m^2\,m^{-2}$ in our study. Szczypta et al. (2011) and Le Moigne (2002) demonstrated that the direct shortwave and long-wave radiative forcing, respectively, are underestimated by approximately 5 % averaged over France. We followed Decharme et al. (2013) in bias-correcting the direct radiative forcing by +5 % for NIT_{bc}.

Table 1. List of experiments. The bias-correct forcing option implies an increase of the direct shortwave and long-wave radiation by 5 %. The SSM outliers removal applies to SSM observations outside the 90 % confidence interval of the model.

Experiment	LAI grassland min ($m^2\,m^{-2}$)	Bias-correct forcing	DA	SSM outliers removal
NIT	0.3	No	No	–
NIT_m	1.2	No	No	–
NIT_{bc}	1.2	Yes	No	–
LDAS1	0.3	No	LAI	–
LDAS2	0.3	No	LAI + SSM	No
$LDAS1_{bc}$	1.2	Yes	LAI	–
$LDAS2_{bc}$	1.2	Yes	LAI + SSM	No
$LDAS2_{QC}$	0.3	No	LAI + SSM	Yes

Three additional experiments in Table 1 explored whether SSM observation outliers, the underestimated LAI minimum or the radiative forcing bias might impact the performance of the DA. The $LDAS2_{QC}$ was equivalent to LDAS2 but with a strict quality control of the SSM observations. The outliers were removed by rejecting observations outside the 90 % confidence interval of the model (as in Eqs. 1 and 2 of Albergel et al., 2010b) after the observations had been rescaled. The $LDAS1_{bc}$ and $LDAS2_{bc}$ experiments were equivalent to LDAS1 and LDAS2 respectively, except they used the NIT_{bc} model. The SSM observations for $LDAS2_{bc}$ were rescaled such that the standard deviation and mean matched those of NIT_{bc}.

The MODCOU hydrogeological model does not account for anthropogenic water management. However, there are many parts of France where anthropogenic water management strongly influences streamflow observations, including the reservoir operations, for hydropower, irrigation, drinking water, flood and low-flow alleviation, and recreational purposes. We used the reference networks of Giuntoli et al. (2012, 2013) to extract a subset of 67 river gauges with low-anthropogenic influence from the original 546 stations, valid for both low and high flows. We compared the results for these 67 stations with the 546 stations in order to determine if the results were affected by the ability of SIM (with or without DA) to simulate anthropogenically influenced streamflow.

2.5 Performance diagnostics

2.5.1 System validation

A system validation was performed by comparing the LAI and WG1 states with the LAI and SSM observations, respectively, for all the simulations and DA experiments. Note that this was not an independent validation of the performance of the system, for which we would have needed independent observations. The rationale was to check the effectiveness of the SEKF, i.e. to examine if it improved the fit between the model simulations and the observations. The fit to the observations was determined by the root mean square difference (RMSD), the correlation coefficient (CC) and the bias.

In addition, Figures S5 and S6 show the histograms of the innovations (difference between the model-predicted observations and the data) and residuals (difference between the analysis and the data). The SSM innovation PDF (probability density function) agrees very well with Kalman theory, since it closely fits the Gaussian distribution. The LAI innovation PDF is also close to its normal fit, but presents a left-tailed distribution. As expected, the standard deviation of residuals is reduced compared to those of innovations. For an optimal filter the innovation time series should be uncorrelated in time. For both SSM and LAI the temporal evolutions of innovations are illustrated in Figs. S7 and S8, respectively. The SSM temporal sequences of innovations are close to a white noise time series (Fig. S7), while the LAI innovations (Fig. S8) are quite strongly correlated over time, which is not optimal.

2.5.2 Validation using SIM

The SIM hydrological model was used to validate the drainage and runoff from ISBA-A-gs by comparing the simulated streamflow from MODCOU with observations. A complete description and validation of SIM can be found in Habets et al. (2008). The first two stages of SIM are the SAFRAN atmospheric forcing and the ISBA-A-gs LSM, which were introduced in Sect. 2.1. The runoff and drainage from ISBA-A-gs are fed into the MODCOU hydrogeological model (Ledoux et al., 1989), which computes the daily evolution of aquifer storages and 3 h river flow forecasts. More than 900 river gauges are simulated with areas ranging from 240 to 112 000 km^2. The temporal and spatial evolution of two aquifers in the Rhône and Seine basins are simulated using a diffusivity equation. The interaction between the rivers and aquifers is modelled and the soil water is routed to the rivers using an isochronism algorithm. The influence of human activity, such as dams and irrigation, is not accounted for by MODCOU. The simulated river discharge from SIM was compared with the observations from 546 river gauges that had data during the period of evaluation (2007–2014). These observations are available from the French hydrographical database (http://www.hydro.eaufrance.fr/, last accessed March 2016). We also analysed the results for the subset of 67 stations with low anthropogenic influence from the original 546 stations. The fit of the average daily river discharge from MODCOU (measured in $m^3\,m^{-3}\,s^{-1}$) to the observations was measured using the Nash efficiency score (Nash and Sutcliffe, 1970). The Nash efficiency can range from $-\infty$ to 1, with 1 corresponding to a perfect match of the model to the observed data and a negative value implying that the model performs worse than a constant model with a value equal to the average of all the observations. Following Habets et al. (2008), we considered an efficiency of 0.6 to be a good score and 0.5 to be a reasonable score. The median Nash scores were calculated for all the stations. The median is a more appropriate metric than the mean as it is less sensitive to extreme outliers and is a better indicator for highly skewed distributions (Moriasi et al., 2007). These issues were present in this study due to some stations being heavily affected by anthropogenic water management or unresolved aquifers, despite most stations being well simulated. The validation period extended from August 2007 to July 2014, with the hydrological year running from August to July.

The SIM domain consists of 9892 grid points, of which 8602 are based in France. The remaining 1290 points are based in mountainous regions bordering the French mainland, including most of Switzerland (see Fig. 2 in Habets et al. (2008) for the full domain). The LSM does not model horizontal exchanges, but MODCOU takes into account horizontal streamflow. Therefore it is important to include these external points in SIM because they impact the streamflow over France, particularly in the Rhône basin in the southeast. However, we only applied the SEKF over the 8602 points in the LDAS France domain. Figure 1 shows a flowchart of SIM and how LDAS France was connected with ISBA-A-gs in SIM. Figure 2 shows the river network used by MODCOU and the 546 stations used to validate the discharge. A map of the subset of 67 stations with low anthropogenic influence can be found in Fig. S1.

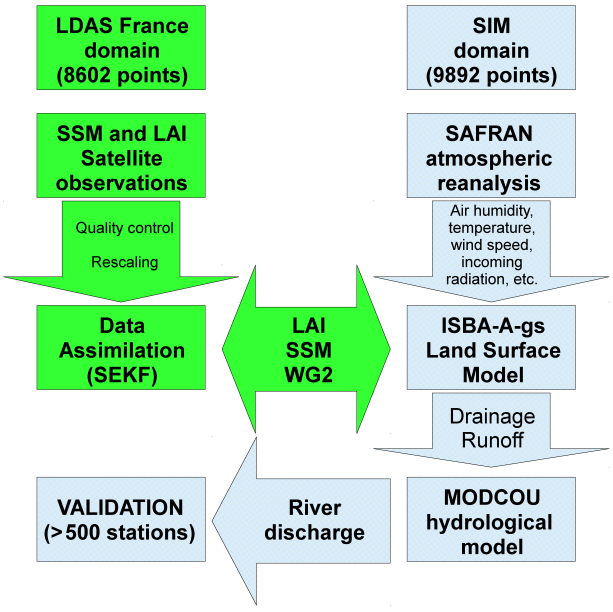

Figure 1. Flowchart of the SIM hydrological model and how LDAS France is connected with SIM.

3 Results

3.1 Impact of model and forcing bias-corrections on SIM

To begin with we examine the influence of the different model simulations (NIT, NIT_m and NIT_{bc}) on the LAI evolution for the four dominant vegetation patches. We can then link the hydrological performance to each simulation. Over France, the four dominant vegetation patches are grasslands (32 %), C3 croplands (24 %), deciduous forests (20 %) and coniferous forests (12 %). Figure 3 shows the monthly averaged LAI model simulations and observations for the grid points that contain at least 50 % of the dominant vegetation types. The 50 % threshold was used because no points contain more than 70 % of deciduous forests, while over 1000 grid points contain at least 50 % of any vegetation type. Table 2 shows the average LAI scores over France (RMSD, CC and bias) for each of the model simulations.

Firstly we examine the LAI performance for the NIT simulation, which dynamically estimates the LAI evolution. Figure 3 shows that the NIT simulation is close to the observations for the deciduous forests (Fig. 3a). However, the growth and senescence phases are delayed for the simulated C3 crops and grasslands (Fig. 3c and d) compared with the observations. Furthermore, the grassland LAI is substantially underestimated by NIT in winter. It is clear in Fig. 3 that imposing this higher minimum LAI value (NIT_m) increases the LAI for grasslands in winter and improves the fit to observations. This is reflected by better scores for NIT_m, reducing (increasing) the RMSD (CC) by about 4 % compared with NIT. Figure 4 shows the average annual LAI minimum over France for the original simulation (NIT), the new simulation (NIT_m) and the GEOV1 data. Figure 4 emphasizes that the LAI minimum is underestimated (compared to the GEOV1 data) over much of France for NIT. By increasing the grassland LAI minimum from 0.3 to 1.2 $m^2\,m^{-2}$, the model agrees much better with the data over most regions. Finally, the benefit of the bias-correction (NIT_{bc}) on LAI is also demonstrated in Fig. 3. The bias-correction has little impact on the LAI of the deciduous and coniferous forest patch types. However, it does reduce the phase errors for both the C3 crops and grassland patches. This results in much better LAI scores, reducing (increasing) the RMSD (CC) by about 10 % compared with NIT_m.

Table 2. Scores for LAI (prognostic variable compared with observations) averaged over 2007–2014. The RMSD and CC stand for root mean square difference and correlation coefficient respectively. The closest fit to the observations is shown in bold font.

Experiment	RMSD ($m^2\,m^{-2}$)	CC	Bias ($m^2\,m^{-2}$)
NIT	1.18	0.56	0.11
NIT_m	1.14	0.58	0.25
NIT_{bc}	1.02	0.63	0.17
LDAS1	0.69	0.82	−0.08
LDAS2	0.71	0.81	−0.04
$LDAS1_{bc}$	**0.63**	**0.84**	−0.04
$LDAS2_{bc}$	0.66	0.83	−0.02
$LDAS2_{QC}$	0.72	0.81	0.02

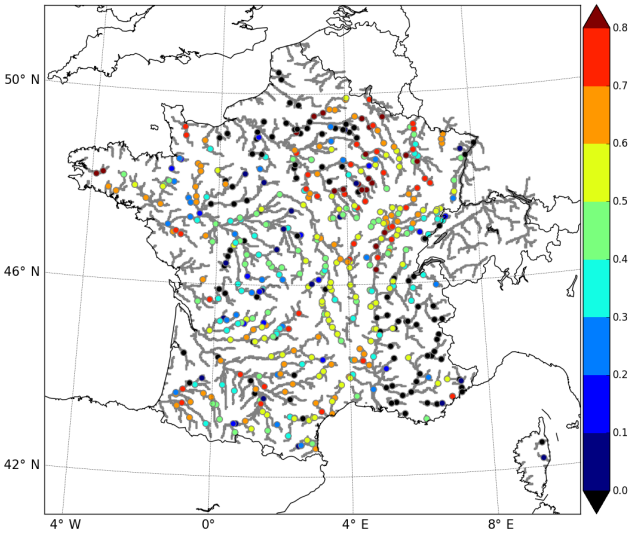

Figure 2. Nash efficiency scores for each station over France for the NIT simulation, calculated over the period 2007–2014. The river network is also shown.

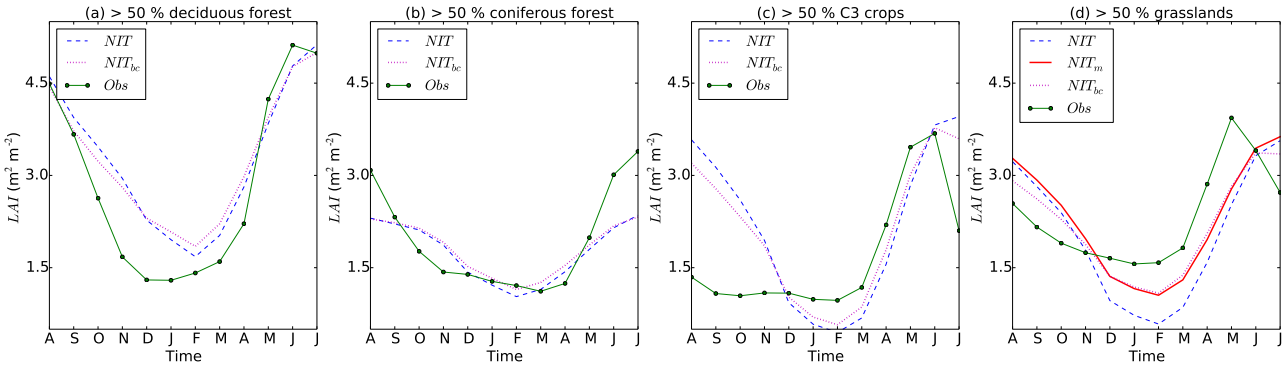

Figure 3. Monthly averaged LAI for the model simulations and for the grid points with at least 50 % of the four dominant vegetation types, averaged over 2007–2014 and averaged over France.

Table 3. Scores for WG1 (prognostic variable compared with observations) averaged over 2007–2014. The RMSD and CC stand for root mean square difference and correlation coefficient respectively. The closest fit to the observations are shown in bold font.

Experiment	RMSD ($m^3\ m^{-3}$)	CC	Bias ($m^3\ m^{-3}$)
NIT	0.051	0.77	0.00
NIT_m	0.049	0.77	0.00
NIT_{bc}	0.051	0.77	0.00
LDAS1	0.049	0.77	0.00
LDAS2	**0.048**	**0.78**	0.00
$LDAS1_{bc}$	0.049	0.77	0.00
$LDAS2_{bc}$	0.049	**0.78**	0.00
$LDAS2_{QC}$	**0.048**	**0.78**	0.00

The WG1 scores for the various simulations are given in Table 3. Recall that the SSM observations are linearly rescaled such that their mean and standard deviation match the NIT model simulation of WG1, which removes any bias already present. Changing the model simulation has little impact on the scores, which suggests that the LAI evolution and the radiative forcing have a relatively small influence on the moisture content of the surface layer.

Next, the Nash efficiency scores for the different model simulations are displayed in Fig. 5a, showing the percentage of gauging stations at efficiency scores between 0 and 1.0. For the NIT simulation, about 26 % of the stations have a score above 0.6 (a good score), 42 % of the stations have a score above 0.5 (a reasonable score) and 79 % of the stations have a positive Nash score. These scores are substantially improved by increasing the LAI minimum and by bias-correcting the radiative forcing. For the NIT_m (NIT_{bc}) simulation, about 31 % (42 %) of stations reach a score of at least 0.6, 48 % (58 %) of stations reach a score of 0.5 or higher and 80 % (83 %) of the stations have a positive score. Table 4 shows the median Nash scores for each simulation. The median Nash scores for NIT are increased by about 9 % for NIT_m and further increased by 18 % for NIT_{bc}. The median discharge ratio between the simulated (Q_s) and observed (Q_o) discharge is also shown for each simulation. A value that is greater (smaller) than 1.0 indicates a positive (negative) bias in the model. NIT has a median discharge ratio of 1.19, which indicates that the simulated streamflow is overestimated by about 20 %. This is reduced to 1.15 by applying the LAI minimum and further reduced to 1.02 by applying the bias-correction. Therefore it appears that the bias in the discharge ratio has an important impact on the Nash score, with larger biases corresponding to smaller Nash scores. This is clarified when comparing the annual median Nash scores (Fig. 6a) with the annual median discharge ratios in Fig. 6b. It seems that the size of the bias in the discharge ratio is negatively correlated with the Nash score, which would explain why NIT_{bc} performs so well. Figure 6c and d show the average annual temperature and rainfall respectively. There does not appear to be a strong correlation between either the temperature or rainfall and the Nash score.

The Nash efficiency for NIT for each station over France is shown in Fig. 2. The river discharge is well simulated over most areas, but the southeast and northern regions have generally negative scores (shown in black). In southeast France this is related to a large number of dams in the Alps, which are not simulated by MODCOU. In northern France, this is linked to a large aquifer that is also not taken into account by MODCOU (see Habets et al., 2008 for details). There are a small number of stations with negative scores elsewhere, which could also be related to anthropogenic water management. The maps show similar patterns for the other simulations (not shown). The vast majority of stations (> 80 %) for NIT_{bc} are improved relative to NIT, including most of the stations with negative scores. A scatter plot of the Nash efficiency scores of NIT and NIT_{bc} for all the stations can be found in Fig. S2a.

Finally, we investigate the influence of the model simulations on the evapotranspiration, drainage and runoff fluxes in order to explain the differences in SIM discharges. Fig-

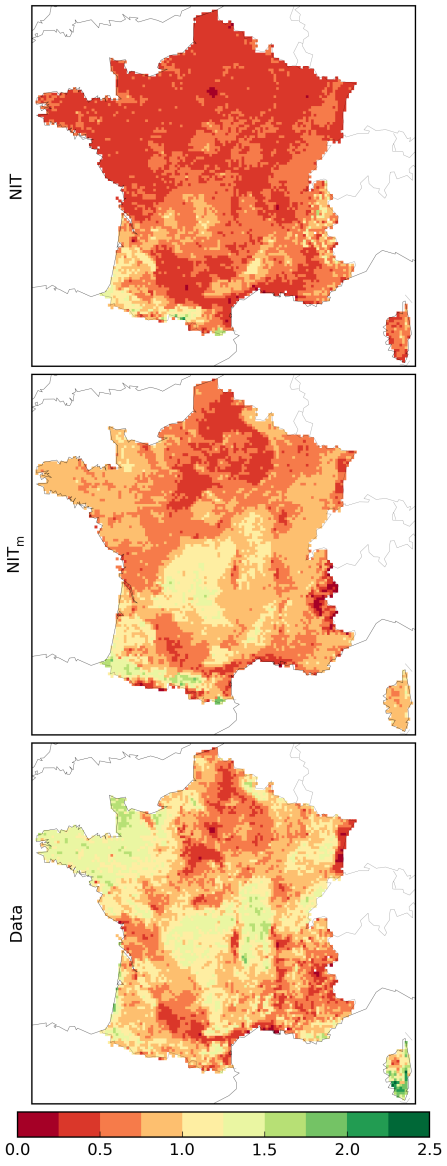

Figure 4. Map showing the average annual LAI minimum (2007–2014) for NIT, NIT$_m$ and the GEOV1 observations (m^2 m^{-2}) over France.

ure 7a–e show the average monthly LAI, WG2, evapotranspiration, drainage and runoff respectively, averaged over France. The NIT$_m$ simulation has a greater average LAI in winter than NIT because the NIT LAI minimum is underestimated. The effect of a higher LAI minimum is to enhance evapotranspiration in winter and spring, which reduces the soil moisture and therefore diminishes the drainage and runoff. The consequence of increased radiative forcing in NIT$_{bc}$ is to further increase evapotranspiration and lower WG2 during much of the year. This substantially reduces drainage and runoff, especially from October to June. These effects are emphasized in Fig. 8a, which shows the difference between the sum of drainage and runoff for the different simulations compared with NIT. The reduced drainage and runoff feeding into the MODCOU hydrogeological model results in less river discharge, which explains the reduced river discharge bias and superior Nash scores for NIT$_m$ and NIT$_{bc}$ relative to NIT in Table 4.

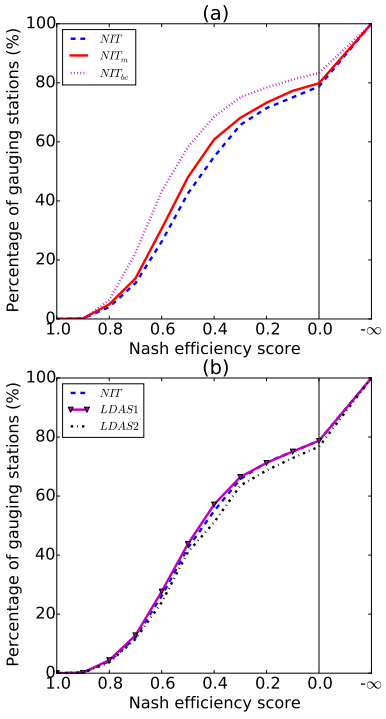

Figure 5. Nash efficiency scores over France for **(a)** the model simulations and **(b)** the DA methods, calculated over the period 2007–2014.

3.2 Impact of DA on SIM

The performance of the DA runs on the LAI and WG1 scores are shown in Tables 2 and 3 respectively. LDAS1 substantially improves the fit of the simulated LAI to the LAI observations compared to NIT. We investigate the influence of DA on the drainage and runoff fluxes in Fig. 7f–j, which is equivalent to Fig. 7a–e except that LDAS1 and LDAS2 are compared with NIT. Figure 7g demonstrates that the assimilation of LAI reduces the LAI phase errors in NIT, indicating that the SEKF is working effectively during much of the year. However, the LAI assimilation with the SEKF does not address the problem of the underestimated LAI in winter, unlike NIT$_m$ in Fig. 7b. Figure 8b shows the differences between the combined drainage and runoff fluxes between NIT and the DA methods. The LAI assimilation has a relatively small influence on the drainage and runoff fluxes in Fig. 8b compared to NIT$_m$ in Fig. 8a. The small positive correction of LAI in spring slightly increases (reduces) evapotranspiration (drainage and runoff) which is cancelled out by the opposite

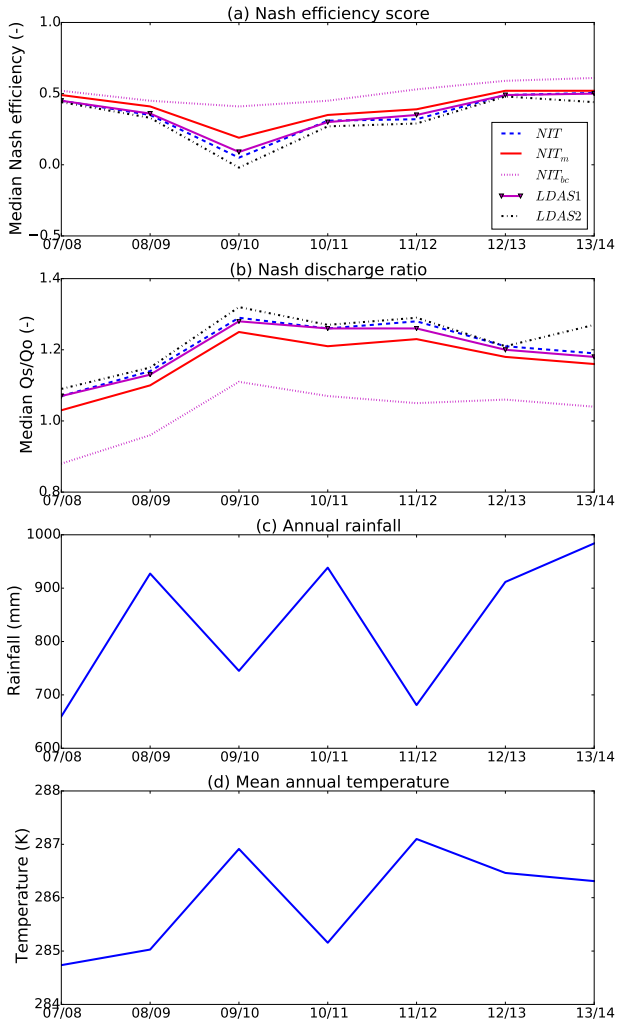

Figure 6. Median annual **(a)** Nash efficiency scores and **(b)** discharge ratio for each experiment. Average annual **(c)** temperature and **(d)** cumulated precipitation.

effect in autumn. Overall, LDAS1 does not greatly modify the discharge ratio or the Nash scores.

The LDAS2 experiment slightly improves the WG1 scores relative to NIT (Table 3). The median Nash discharge scores are degraded by about 7 % for LDAS2 compared to NIT (Fig. 5b and Table 4) and the positive bias in the discharge ratio is increased by about 2 % (Table 4). The reason for this is that LDAS2 has a higher average WG2 relative to NIT (Fig. 7f), which translates to increased drainage and runoff for LDAS2. This is emphasized by comparing the combined drainage and runoff for LDAS2 relative to NIT in Fig. 8b. The extra water in the rivers exacerbates the Nash discharge bias already present in NIT, resulting in degraded Nash efficiency scores. The LDAS2 scores are degraded for about 70 % of the stations relative to the NIT simulation and a scatter plot of the scores for all the stations can be found in Fig. S2b.

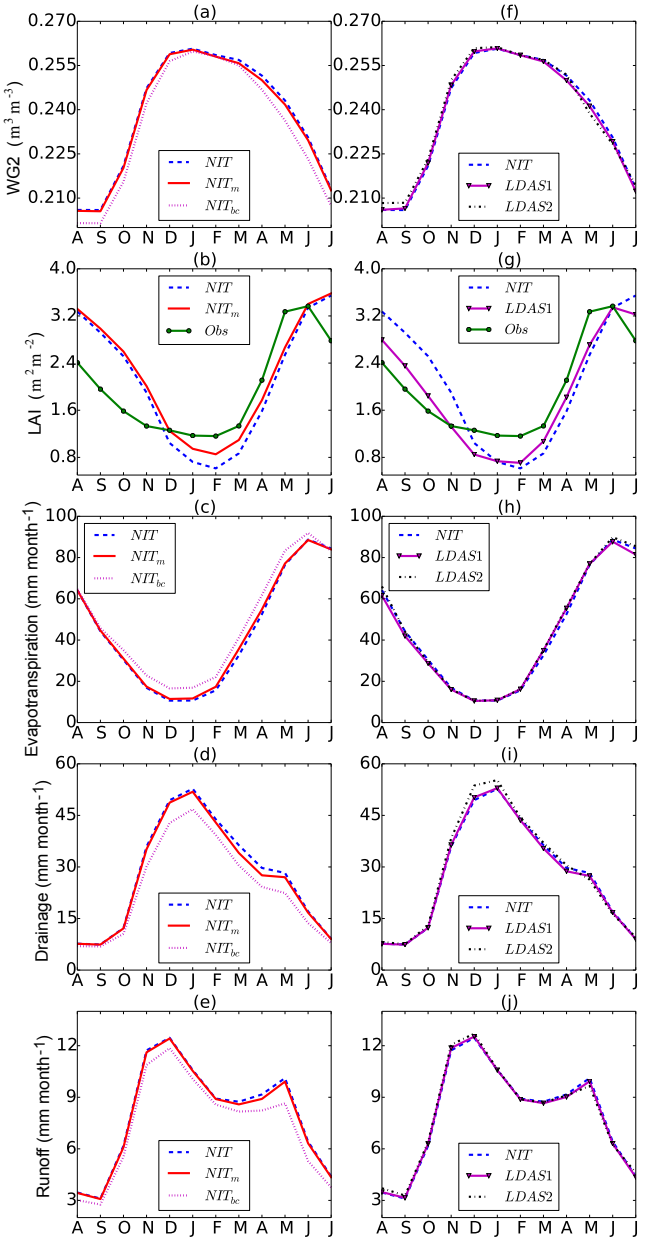

Figure 7. Average monthly **(a)** WG2 and **(b)** LAI, and monthly cumulative **(c)** evapotranspiration, **(d)** drainage and **(e)** runoff for NIT and the other model simulations. Plots **(f–j)** show NIT and the DA analyses for the equivalent variables as in **(a–e)**. Results are all averaged over the period 2007–2014 and averaged over France.

The neutral impact of LDAS1 and the detrimental influence of LDAS2 on the soil moisture fluxes is explained in the following section by examining the observation operator Jacobians.

Table 4. Median Nash efficiency (NE) and discharge ratio (Q_s / Q_o) scores over the 546 river gauges over France and for the subset of 67 gauges with low anthropogenic influence, calculated over 2007–2014. Also shown are the percentage of stations with a Nash score above 0.6. The best scores are shown in bold font.

Experiment	NE for 546/67 stations	Discharge ratio for 546/67 stations	% stations with NE > 0.6 for 546/67 stations
NIT	0.44/0.48	1.19/1.16	26 %/44 %
NIT_m	0.48/0.54	1.15/1.12	30 %/48 %
NIT_{bc}	**0.56**/**0.60**	**1.02**/**0.99**	**42** %/**59** %
LDAS1	0.44/0.48	1.18/1.15	27 %/44 %
LDAS2	0.41/0.45	1.21/1.18	23 %/40 %
$LDAS1_{bc}$	**0.56**/**0.60**	**1.02**/**1.00**	**42** %/**57** %
$LDAS2_{bc}$	0.53/0.54	1.08/1.06	38 %/53 %
$LDAS2_{QC}$	0.40/0.45	1.21/1.18	21 %/39 %

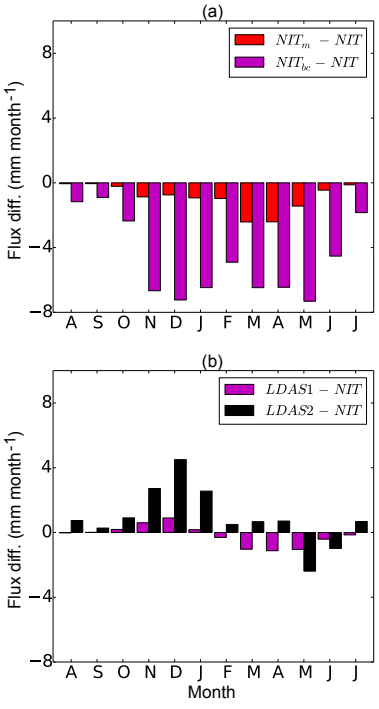

Figure 8. Monthly combined drainage + runoff flux differences between **(a)** NIT and the other model simulations and **(b)** NIT and the DA analyses averaged over the period 2007–2014 and over France.

3.3 Examining the SEKF Jacobians

The SEKF observation operator Jacobians are governed by the physics of the model. Their examination is important in order to understand the SEKF performance. The LAI increments for LDAS1 are mainly driven by the $\frac{\partial \mathrm{LAI}}{\partial \mathrm{LAI}}$ Jacobian. The behaviour of the $\frac{\partial \mathrm{LAI}}{\partial \mathrm{LAI}}$ Jacobian values for ISBA-A-gs was investigated by Rüdiger et al. (2010). Their behaviour can be split into three distinct types, which depend on atmospheric conditions. The type "O" Jacobian is strictly equal to zero and occurs mainly in winter when the vegetation is dormant. In this case the LAI will be kept at its default model minimum. The type "A" Jacobian represents a fraction between zero and one and is correlated with the LAI value itself. It occurs during periods of vegetation growth, i.e. predominantly in spring. The type "B" Jacobian is equal to 1.0 and takes place during periods of low vegetation growth or high mortality, which occur mainly in autumn. The grassland Jacobians are plotted for LDAS1 in Fig. 9 for a particular point in southwest France (43.35° N, 1.30° E). Also plotted in the same graph are the LAI values themselves, with the minimum indicated by the red line. Indeed, the type O Jacobians tend to occur in winter, during which time the LAI returns to its minimum value of 0.3 $\mathrm{m}^2\,\mathrm{m}^{-2}$. The type A and B Jacobians tend to occur in spring and autumn respectively. These findings are in agreement with Fig. 4 of Rüdiger et al. (2010). The LAI performance for LDAS1 can now be explained by these Jacobian values. Figure 7g shows that during the winter the lowest LAI values are barely corrected by LDAS1 because, as shown in Fig. 9, the LAI is frequently forced back to its minimum value (type O Jacobians). During the spring there is a small correction (type A Jacobians) and during the autumn there is a much larger correction (type B Jacobians). Hence the LDAS1 is able to correct the LAI phase errors to some extent, but LDAS1 is unable to correct the LAI minimum in winter. The seasonal imbalances in the LAI Jacobian can also explain the negative bias in Table 2. Since most of the drainage and runoff is present in winter and spring, the assimilation of LAI has little influence on SIM.

The $\frac{\partial \mathrm{LAI}}{\partial \mathrm{WG2}}$ Jacobian has generally positive values, since an increase in water content in the soil generally enhances photosynthesis and plant growth (not shown). However, this term is close to zero from about November to March while the vegetation is dormant. Therefore it does not substantially influence the LAI minimum in winter. There is no evidence that it leads to long-term increases in WG2 or results in increased drainage and/or runoff for LDAS2.

The WG2 analysis increments for LDAS2 are largely driven by the $\frac{\partial \mathrm{WG1}}{\partial \mathrm{WG2}}$ Jacobian. A scatter plot of these Jacobian values against the WG1 variable is shown in Fig. 10 for the same point as Fig. 9 in southwest France. The density of the points is derived from the kernel density estimation of Scott (1992). There are two dense regions when WG1 is equal to 0.15 and 0.30 $\mathrm{m}^3\,\mathrm{m}^{-3}$, which occur because WG1 is a thin layer, and therefore most of the time it is either dry or close to saturation. The WG1 and $\frac{\partial \mathrm{WG1}}{\partial \mathrm{WG2}}$ values are negatively correlated, with larger values of WG1 corresponding to smaller values of $\frac{\partial \mathrm{WG1}}{\partial \mathrm{WG2}}$. This implies that when rain is detected in the model but not in the SSM observations, the analysis increment will be smaller than when the rain is missed by the model but detected by the observations. Indeed, the average WG2 analysis increment for a positive innovation is $0.7 \times 10^{-3}\,\mathrm{m}^3\,\mathrm{m}^{-3}$, while the average increment for a negative innovation is $-0.5 \times 10^{-3}\,\mathrm{m}^3\,\mathrm{m}^{-3}$. This imbal-

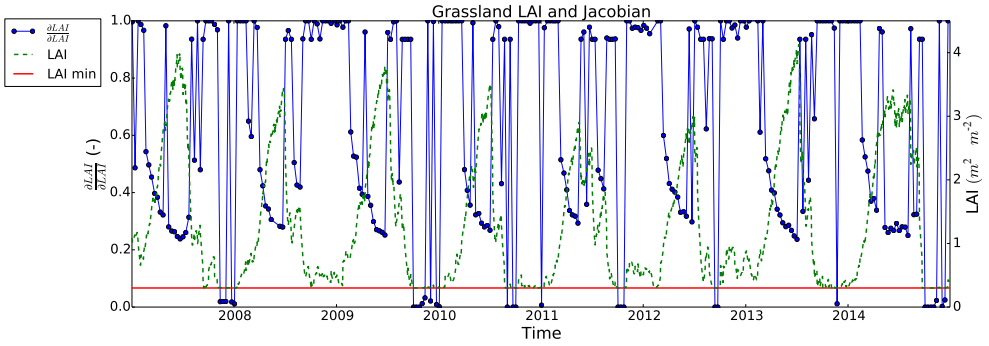

Figure 9. Time evolution of the LDAS1 $\frac{\partial \mathrm{LAI}}{\partial \mathrm{LAI}}$ Jacobian, together with the LAI analysis and the minimum LAI model parameter for the grassland patch at a point in southwest France (43.35° N, 1.30° E).

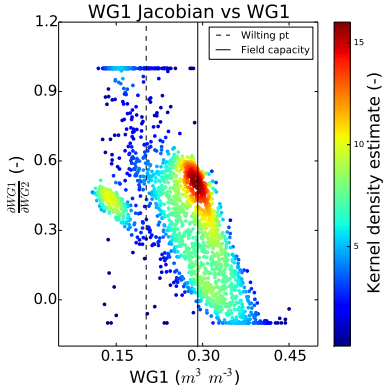

Figure 10. Scatter plot of WG1 against the LDAS2 $\frac{\partial \mathrm{WG1}}{\partial \mathrm{WG2}}$ Jacobian for the grassland patch at the same point as Fig. 9.

ance in the analysis increments leads to a net uptake of water in WG2, which induces the positive bias in the SIM river discharge. This problem was already highlighted by Draper et al. (2011). The Jacobians exhibited similar patterns of behaviour for other vegetation types than grasslands and across other points in France, albeit with different magnitudes (not shown).

3.4 Additional experiments

Additional experiments were performed to examine whether the poor performance of the SEKF was related to other factors than the Jacobians, namely the quality control of the observations, the underestimated LAI minimum or the bias in the atmospheric forcing. It is evident in Tables 2 to 4 that applying the additional quality control of the SSM observations ($\mathrm{LDAS2_{QC}}$) does not substantially modify the LAI, WG1 or Nash discharge scores compared to LDAS2, despite removing about 10 % of the SSM observations. Figure 11a shows only small differences in the Nash efficiency percentages between LDAS2 and $\mathrm{LDAS2_{QC}}$. As expected, the $\mathrm{LDAS1_{bc}}$ and $\mathrm{LDAS2_{bc}}$ experiments improved on the LAI scores of LDAS1 and LDAS2 (Tables 2 and 4), but did not improve on the WG1 scores in Table 3. These changes are a similar order of magnitude to the improvement of $\mathrm{NIT_{bc}}$ over NIT. In terms of discharge Nash efficiency scores, $\mathrm{LDAS1_{bc}}$ performed similarly to $\mathrm{NIT_{bc}}$ and LDAS2 performed substantially worse than $\mathrm{NIT_{bc}}$ (Table 4). The Nash efficiency percentages are shown in Fig. 11(b). The comparison between $\mathrm{LDAS1_{bc}}$ and $\mathrm{LDAS2_{bc}}$ with $\mathrm{NIT_{bc}}$ in Fig. 11b is analogous to the comparison between LDAS1 and LDAS2 with NIT in Fig. 5b.

The scores for the subset of 67 stations with low anthropogenic influence are also shown in Table 4. The scores for this subset are improved relative to the 546 stations in Table 4, as expected. In particular, the percentage of stations with good scores (Nash efficiency > 0.6) is greatly increased. For the interested reader, scatter plots of the Nash scores for the 67 stations are shown in Fig. S3. The discharge bias is also slightly smaller for the stations with low anthropogenic influence relative to the 546 stations. This suggests that a small part of the positive bias in the discharge ratio of the NIT simulation for the 546 stations could be attributed to abstractions not being accounted for, such as drinking water or irrigation. However, most of the discharge bias in the NIT simulation is still present in the 67 stations with low anthropogenic influence. Moreover, the relative performances of the experiments are very similar. Therefore, the conclusions of the experiments are not affected by the ability of SIM (with or without DA) to simulate anthropogenically influenced streamflow. These results confirm that the inability of the SEKF to improve the soil moisture fluxes comes mostly from the SEKF Jacobians.

4 Discussion

Previous work by Muñoz Sabater et al. (2007) and Fairbairn et al. (2015) clearly demonstrated that the assimilation of SSM observations with an SEKF can improve WG2 with the three-layer ISBA-A-gs model. Barbu et al. (2014) also demonstrated that the assimilation of LAI reduces phase errors in the modelled LAI evolution. However, in this

work we showed that the SEKF has little influence on the drainage and runoff fluxes when assimilating LAI observations (LDAS1 experiment). Furthermore, the SEKF actually degrades these fluxes when assimilating SSM and LAI observations (LDAS2 experiment). The differences in these findings are due to the nonlinear interactions in LSMs which can cause the assimilation of one state variable to be detrimental to other soil moisture processes (Walker and Houser, 2005). The poor results for LDAS1 and LDAS2 can be explained by model errors, atmospheric forcing errors and model nonlinearities near the soil moisture wilting point and field capacity thresholds, none of which are captured by the SEKF observation operator Jacobians.

4.1 Could LAI assimilation be improved?

In LDAS1, the seasonal variability in the analysis LAI increments was uneven, with large negative increments in late summer–autumn and small positive increments in winter–spring. This occurred because the LAI Jacobian $\left(\frac{\partial \mathrm{LAI}}{\partial \mathrm{LAI}}\right)$ was frequently equal to zero during winter and therefore the LAI remained at its incorrect minimum value after the analysis update. Moreover, LAI is only assimilated every 10 days so the model LAI would drift back to its underestimated minimum value between cycles. Consequently, the average LAI analysis was negatively biased. These Jacobian values are physically sensible, since the vegetation is dependent on the atmospheric conditions and is often dormant during the winter period. The problem is related to the lack of a model error term in the SEKF.

The lowest LAI values could be corrected with a full EKF and a model error term, but it would be complicated to parametrize the model-error covariance matrix because the LAI minimum is linked to several factors concerning the atmospheric conditions and the vegetation type. A short-term solution to the underestimated LAI minimum was demonstrated in the experiments, which was to set a higher LAI minimum parameter in the model based on observations. However, it would be more sensible in the long-term to resolve the underlying issues with the model physics. A thorough comparison of the ISBA-A-gs-simulated LAI with both SPOT-VGT (used in our experiments) and MODIS data over southwest France was performed by Brut et al. (2009). They did notice significant discrepancies between all three data sets, suggesting that there is significant uncertainty in both the model and the observations. However, they also noticed that the modelled LAI of the C3 natural herbaceous (grasslands) and/or C3 crops had a delayed onset relative to both satellite products (see Fig. 4 in Brut et al., 2009). They found that this was particularly problematic for grasslands in mountainous regions. By comparing the data with in situ measurements, they found that the generic temperature response of photosynthesis used in the model is not appropriate for plants adapted to the cold climatic conditions of the mountainous

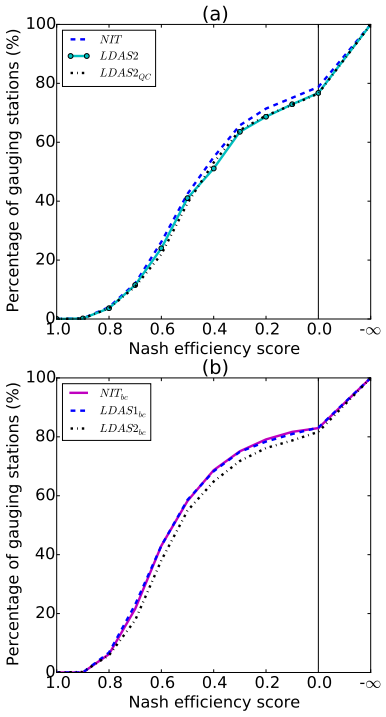

Figure 11. Average Nash efficiency scores over France for **(a)** the NIT, LDAS2 and $\mathrm{LDAS2_{QC}}$ experiments, and **(b)** the $\mathrm{NIT_{bc}}$, $\mathrm{LDAS1_{bc}}$ and $\mathrm{LDAS2_{bc}}$ experiments.

areas. This problem was also linked to a prolonged LAI minimum in the model relative to the observations. Lafont et al. (2012) found similar issues when comparing the same products over France. Indeed, Fig. 4 in our study shows that the NIT LAI minimum was particularly underestimated in the grassland areas of the Massif Central mountains in central France, but not so much in lower regions further north. Finally, these problems could explain the delayed onset and underestimated LAI minimum for both grasslands and C3 crops in Fig. 3 in our study.

It should be recognized that errors in the modelled LAI are not just present over grasslands, but also over other vegetation types. Figure 3 shows that there are significant discrepancies between the model and the observations for C3 crops and deciduous forests as well. Given that these discrepancies vary substantially between different vegetation types, it is not optimal to assimilate a grid point averaged observation. This issue is currently addressed by disaggregating the LAI for each patch individually.

Finally, as already mentioned, LAI is assimilated every 10 days. LAI data availability could be improved using higher spatial and temporal resolution products in order to limit the impact of clouds.

4.2 Why does SSM assimilation degrade river discharges?

It is important to point out that it is physically sensible for WG1 to decouple from WG2 during precipitation events. The precipitation forcing leads to a saturation of the surface layer and subsequently WG1 becomes less dependent on WG2. The degradation of drainage and runoff can be caused by limitations in the SEKF, in the land surface model and in the data.

Firstly, as recognized by Draper et al. (2011), an important problem is that the SEKF is not designed to capture the uncertainty in the model and the precipitation forcing, which should increase during precipitation events and therefore compensate for the smaller Jacobians. The SAFRAN precipitation forcing performs well for a mesoscale analysis and has a higher spatial resolution than global satellite products such as ERA-interim (Quitana-Ségui et al., 2008; Vidal et al., 2010). However, by design the precipitation is assumed to be homogeneous over 615 specified climate zones. Errors are therefore introduced from the spatial heterogeneity of the precipitation, particularly in mountainous regions (Quitana-Ségui et al., 2008).

Secondly, the three-layer ISBA model has strong nonlinearities near the soil moisture thresholds, some of which lead to unrealistic behaviours of the model Jacobians. During dry conditions in summer, the SEKF $\frac{\partial WG1}{\partial WG2}$ Jacobian can be excessive. This is linked to a rapid increase in transpiration when water is added to WG2 following dry conditions (Draper et al., 2009; Fairbairn et al., 2015). The origin of this nonlinearity is partly related to an unrealistic feature of the surface energy balance. One single surface temperature is used to represent the vegetation and the surface layer, which causes the transpiration to increase too quickly after water is added to WG2 (Draper et al., 2009; Mahfouf, 2014). This problem could be relieved to some extent by introducing the new version of ISBA with a multiple energy balance (Boone et al., 2017) and by using a multi-layer diffusion model (ISBA-DIF, Decharme et al., 2011).

Lastly, regarding observations, the current ASCAT product is affected by vegetation (Vreugdenhill et al., 2016) and a seasonal cumulative distribution function (CDF) matching is needed in DA systems assimilating ASCAT SSM. This procedure is, however, sub-optimal. A solution to this problem is to go towards the implementation of an observation operator in order to assimilate the backscattering coefficients directly. In this way, the vegetation information content in the ASCAT signal could be used to analyse vegetation biomass and would also provide information for the analysis of root-zone soil moisture, in addition to the microwave soil moisture signal.

4.3 Could more sophisticated DA methods improve SSM assimilation?

The presence of the uncertainties in the model and in the forcing could more easily be addressed with an EnKF than an SEKF because an EnKF can stochastically represent model and precipitation errors (Maggioni et al., 2012; Carrera et al., 2015). Fairbairn et al. (2015) found that an EnKF with a simple stochastic rainfall error estimation demonstrated similar WG2 scores to the SEKF over 12 sites in southwest France (validated using in situ observations). Both methods were affected by nonlinearity problems.

There are DA methods, such as particle filters, designed to handle model nonlinearities. Moradkhani et al. (2012) demonstrated that good results on a hydrological model could be achieved with a particle filter with about 200 members. However, it is substantially more computationally expensive than an EnKF, which typically requires about 20 members to overcome sampling error problems for LSMs (Maggioni et al., 2012; Carrera et al., 2015; Fairbairn et al., 2015). Therefore we intend to test an EnKF over France using the same validation framework used in this study.

5 Conclusions

This study assessed the impact on streamflow simulations of assimilating SSM and LAI observations into the ISBA-A-gs LSM. The drainage and runoff outputs were used to force the MODCOU hydrogeological model and were validated by comparing the simulated streamflow with over 500 river-gauge observations over France over several years. To our knowledge, this is the first article to examine the impact of LAI assimilation on streamflow simulations using a distributed hydrological model. The validation is robust due to the large number of river gauge observations employed and the long evaluation period (2007–2014). The results from this study could also have ramifications for flood warning accuracy since SIM is used operationally by Meteo-France as a tool for flood forecasting. Furthermore, this study highlights the importance of systematic model and/or forcing deficiencies on the streamflow simulations. Reasons for not obtaining improvements in discharge simulations are related to model deficiencies, model nonlinearities and the set-up of the assimilation system.

Increasing the LAI minimum parameter resulted in greater evapotranspiration in winter–spring, and bias-correcting the radiative forcing increased evapotranspiration during much of the year. Both corrections effectively reduced the positive bias in the drainage and/or runoff fluxes and substantially improved the Nash efficiency scores. Although DA is not theoretically designed to correct systematic model deficiencies, it was found that assimilating only LAI observations substantially reduced the LAI phase errors in the model. However, this induced a net negative bias in the LAI analysis relative to

the observations. Given that drainage and runoff occurs predominantly in late winter and spring, the LAI assimilation had a negligible impact on these fluxes.

Assimilating SSM resulted in spurious increases in drainage and runoff, which degraded the SIM discharge Nash efficiency.

An issue in DA experiments was the underlying assumption made by the SEKF that the model is perfect. Allowing for model and atmospheric forcing errors could more easily be addressed with an EnKF method than the SEKF, although both methods are affected by nonlinearity issues. In the future we will test the EnKF using a similar validation employed in this study. Regarding LAI assimilation, the SEKF assimilates the LAI observations by aggregating the different vegetation patches in each grid box. This approach is not optimal because each vegetation type exhibits unique seasonal variability. Given the high resolution of LAI observations (1 km), work is underway to disaggregate the observations.

While the ISBA LSM is well established and is used operationally at Meteo-France, this study has helped us to identify some limitations that need to be addressed. A new multilayer diffusion model should improve representation of the coupling between the surface and root-zone soil moisture. Furthermore, a new multiple energy balance version should decouple the bare soil evaporation and the transpiration processes that lead to an unphysical link in ISBA between surface and deep soil moisture. Previous research has demonstrated that the generic temperature response of photosynthesis used in the model is not appropriate for plants adapted to the cold climatic conditions of the mountainous areas. This is consistent with the phase errors and the underestimated grassland LAI minimum in our study. Solving this problem would presumably increase the LAI minimum in winter, which would be more sensible than simply fitting the LAI minimum to observations. Finally, the LDAS should benefit from further improvement of the satellite-derived LAI and SSM. Using an observation operator for the ASCAT backscattering coefficients would permit accounting for the vegetation information content in the ASCAT signal.

Data availability. The SAFRAN data are available to the research community through the HYMEX database (http://mistrals.sedoo.fr/HyMeX/, Meteo-France, 2015). The satellite-derived observations are freely accessible from the Copernicus Global Land Service (http://land.copernicus.eu/global/, Copernicus, 2015). Streamflow data are available from the Global Runoff Data Centre (GRDC) (http://www.bafg.de/GRDC/EN/Home/homepage_node.html, GRDC, 2015) and identified in the GRDC as the French contribution to the "Climate sensitive stations".

The Supplement related to this article is available online at doi:10.5194/hess-21-2015-2017-supplement.

Competing interests. The authors declare that they have no conflict of interest.

Acknowledgements. This work is a contribution to the IMAGINES (grant agreement 311766) project, co-funded by the European Commission within the Copernicus initiative in FP7. The work was also funded by the EUMETSAT H-SAF service. Discussions with Patrick Le Moigne were useful for understanding the SIM hydrological model. Useful feedback was also obtained through discussions with DA scientists at the Met Office. We would like to thank the two anonymous reviewers for their constructive comments. We would also like to thank Jean-Philippe Vidal from IRSTEA for his useful comments and suggestions regarding anthropogenic water management in the SIM hydrological model.

Edited by: W. Wagner
Reviewed by: four anonymous referees

References

Albergel, C., Rüdiger, C., Pellarin, T., Calvet, J.-C., Fritz, N., Froissard, F., Suquia, D., Petitpa, A., Piguet, B., and Martin, E.: From near-surface to root-zone soil moisture using an exponential filter: an assessment of the method based on in-situ observations and model simulations, Hydrol. Earth Syst. Sci., 12, 1323–1337, doi:10.5194/hess-12-1323-2008, 2008.

Albergel, C., Calvet, J.-C., de Rosnay, P., Balsamo, G., Wagner, W., Hasenauer, S., Naeimi, V., Martin, E., Bazile, E., Bouyssel, F., and Mahfouf, J.-F.: Cross-evaluation of modelled and remotely sensed surface soil moisture with in situ data in southwestern France, Hydrol. Earth Syst. Sci., 14, 2177–2191, doi:10.5194/hess-14-2177-2010, 2010.

Albergel, C., de Rosnay, P., Balsamo, G., Isaksen, L., and noz Sabater, J. M.: Soil Moisture Analyses at ECMWF: Evaluation Using Global Ground-Based In Situ Observations, J. Hydrometeorol., 13, 1442–1460, doi:10.1175/JHM-D-11-0107.1, 2012.

Aubert, D., Loumagne, C., and Oudin, L.: Sequential Assimilation of Soil Moisture and Streamflow Data in a Conceptual Rainfall-Runoff Model, J. Hydrol., 280, 145–161, 2003.

Barbu, A. L., Calvet, J.-C., Mahfouf, J.-F., Albergel, C., and Lafont, S.: Assimilation of Soil Wetness Index and Leaf Area Index into the ISBA-A-gs land surface model: grassland case study, Biogeosciences, 8, 1971–1986, doi:10.5194/bg-8-1971-2011, 2011.

Barbu, A. L., Calvet, J.-C., Mahfouf, J.-F., and Lafont, S.: Integrating ASCAT surface soil moisture and GEOV1 leaf area index into the SURFEX modelling platform: a land data assimilation application over France, Hydrol. Earth Syst. Sci., 18, 173–192, doi:10.5194/hess-18-173-2014, 2014.

Baret, F., Weiss, M., Lacaze, R., Camacho, F., Makhmared, H., Pacholczyk, P., and Smetse, B.: GEOV1: LAI and FAPAR essential climate variables and FCOVER global time series capitalizing over existing products. Part 1: Principles of development and production, Remote Sens. Environ., 137, 299–309, 2013.

Bartalis, Z., Wagner, W., Naeimi, V., Hasenauer, S., Scipal, K., Bonekamp, H., Figa, J., and Anderson, C.: Initial soil moisture retrievals from the METOP-A Advanced

Scatterometer (ASCAT), Geophys. Res. Lett., 34, L20401, doi:10.1029/2007GL031088, 2007.

Boone, A., Calvet, J.-C., and Noilhan, J.: Inclusion of a Third Soil Layer in a Land Surface Scheme Using the Force-Restore Method, J. Appl. Meteor., 38, 1611–1630, 1999.

Boone, A., Samuelsson, P., Gollvik, S., Napoly, A., Jarlan, L., Brun, E., and Decharme, B.: The interactions between soil-biosphere-atmosphere land surface model with a multi-energy balance (ISBA-MEB) option in SURFEXv8 – Part 1: Model description, Geosci. Model Dev., 10, 843–872, doi:10.5194/gmd-10-843-2017, 2017.

Brut, A., Rüdiger, C., Lafont, S., Roujean, J.-L., Calvet, J.-C., Jarlan, L., Gibelin, A.-L., Albergel, C., Le Moigne, P., Soussana, J.-F., Klumpp, K., Guyon, D., Wigneron, J.-P., and Ceschia, E.: Modelling LAI at a regional scale with ISBA-A-gs: comparison with satellite-derived LAI over southwestern France, Biogeosciences, 6, 1389–1404, doi:10.5194/bg-6-1389-2009, 2009.

Calvet, J.-C. and Noilhan, J.: From Near-Surface to Root-Zone Soil Moisture Using Year-Round Data, J. Hydrometeorol., 1, 393–411, 2000.

Calvet, J.-C., Noilhan, J., Roujean, J.-L., Bessemoulin, P., Cabelguenne, M., Olioso, A., and Wigneron, J.-P.: An interactive vegetation SVAT model tested against date from six contrasting sites, Agr. Forest Meteorol., 126, 73–95, 1998.

Candy, B., Bovis, K., Dharssi, I., and Macpherson, B.: Development of an Extended Kalman Filter for the Land Surface, Technical report, Met Office, Exeter, UK, 2012.

Carrera, M., Bélair, S., and Bilodeau, B.: The Canadian Land Data Assimilation System (CaLDAS): Description and Synthetic Evaluation Study, J. Hydrometeorol., 16, 1293–1294, doi:10.1175/JHM-D-14-0089.1, 2015.

Clark, M., Rupp, D., Woods, R., Zheng, X., Ibbitt, R., Slater, A., Schmidt, J., and Uddstrom, M.: Hydrological data assimilation with the ensemble Kalman filter: Use of streamflow observations to update states in a distributed hydrological model, Adv. Water Resour., 31, 1309–1324, 2008.

Copernicus: LAI GEOV1 and SWI-001 version 2, available at: http://land.copernicus.eu/global/ (last access: April 2017), 2015.

Courtier, P., Freydier, C., Geleyn, J.-F., Rabier, F., and Rochas, M.: The ARPEGE model development at Meteo-France, in: Proc. ECMWF Seminar on Numerical Methods in Atmospheric Models, vol. 2, pp. 193–232, ECMWF, Shinfield Park, Reading, 2001.

Crow, W. and Wood, E.: The assimilation of remotely sensed soil brightness temperature imagery into a land surface model using Ensemble Kalman filtering, Adv. Water Resour., 26, 137–149, 2003.

Deardorff, J.: A paramaterization of ground surface moisture for use in atmospheric prediction models, J. Appl. Meteorol., 16, 1182–1185, 1977.

Decharme, B., Boone, A., Delire, C., and Noilhan, J.: Local evaluation of the Interaction between Soil Biosphere Atmosphere soil multilayer diffusion scheme using four pedotransfer functions, J. Geophys. Res., 116, D20126, doi:10.1029/2011JD016002, 2011.

Decharme, B., Martin, E., and Faroux, S.: Reconciling soil thermal and hydrological lower boundary conditions in land surface models, J. Geophys. Res.-Atmos., 118, 7819–7834, doi:10.1002/jgrd.50631, 2013.

Dee, D.: Bias and data assimilation, Q. J. Roy. Meteor. Soc., 131, 3323–3343, doi:10.1256/qj.05.137, 2005.

de Jeu, R. A. M., Wagner, W., Holmes, T. R. H., Dolman, A., de Giesen, N. C., and Friesen, J.: Global soil moisture patterns observed by space borne microwave radiometers and scatterometers, Surv. Geophys., 29, 399–420, 2008.

de Rosnay, P., Drusch, M., Vasiljevic, D., Balsamo, G., Albergel, C., and Isaksen, L.: A simplified Extended Kalman Filter for the global operational soil moisture analysis at ECMWF, Q. J. Roy. Meteor. Soc., 139, 1199–1213, doi:10.1002/qj.2023, 2013.

Draper, C., Mahfouf, J.-F., and Walker, J.: An EKF assimilation of AMSR-E soil moisture into the ISBA surface scheme, J. Geophys. Res., 114, D20104, doi:10.1029/2008JD011650, 2009.

Draper, C., Mahfouf, J.-F., Calvet, J.-C., Martin, E., and Wagner, W.: Assimilation of ASCAT near-surface soil moisture into the SIM hydrological model over France, Hydrol. Earth Syst. Sci., 15, 3829–3841, doi:10.5194/hess-15-3829-2011, 2011.

Draper, C., Reichle, R., Lannoy, G. D., and Liu, Q.: Assimilation of passive and active microwave soil moisture retrievals, Geophys. Res. Lett., 39, L04401, doi:10.1029/2011GL050655, 2012.

Draper, C., Reichle, R., de Jeu, R., Naeimi, V., Parinussa, R., and Wagner, W.: Estimating root mean square errors in remotely sensed soil moisture over continental scale domains, Remote Sens. Environ., 137, 288–298, doi:10.1016/j.rse.2013.06.013, 2013.

Drusch, M., Wood, M., and Gao, H.: Observation operators for the direct assimilation of TRMM Microwave Imager retrieved soil moisture, Geophys. Res. Lett, 32, L15403, doi:10.1029/2005GL023623, 2005.

Durand, Y., Brun, E., Mérindol, L., Gilbert, G., Bernard, L., and Martin, E.: A meteorological estimation of relevant parameters for snow models, Ann. Glaciol., 18, 65–71, 1993.

ECMWF: Annual Report 2015, ECMWF website, http://www.ecmwf.int/sites/default/files/elibrary/2016/16478-annual-report-2015.pdf, last access: July 2016.

Entekhabi, D., Njoku, E. G., O'Neill, P. E., Kellogg, K. H., Crow, W. T., Edelstein, W. N., Entin, J. K., Goodman, S. D., Jackson, T. J., Johnson, J., Kimball, J., Piepmeier, J. R., Koster, R. D., Martin, N., McDonald, K. C., Moghaddam, M., Moran, S., Reichle, R., Shi, J. C., Spencer, M. W., Thurman, S. W., Tsang, L., and Van Zyl, J.: The Soil Moisture Active Passive (SMAP) Mission, Proc. IEEE, 98, 704–716, 2010.

Fairbairn, D., Barbu, A. L., Mahfouf, J.-F., Calvet, J.-C., and Gelati, E.: Comparing the ensemble and extended Kalman filters for in situ soil moisture assimilation with contrasting conditions, Hydrol. Earth Syst. Sci., 19, 4811–4830, doi:10.5194/hess-19-4811-2015, 2015.

Faroux, S., Kaptué Tchuenté, A. T., Roujean, J.-L., Masson, V., Martin, E., and Le Moigne, P.: ECOCLIMAP-II/Europe: a twofold database of ecosystems and surface parameters at 1 km resolution based on satellite information for use in land surface, meteorological and climate models, Geosci. Model Dev., 6, 563–582, doi:10.5194/gmd-6-563-2013, 2013.

Gibelin, A.-L., Calvet, J.-C., Roujean, J.-L., Jarlan, L., and Los, S.: Ability of the land surface model ISBA-A-gs to simulate leaf area index at the global scale: Comparison with satellites products, J. Geophys. Res., 111, D18102, doi:10.1029/2005JD006691, 2006.

Giuntoli, I., Renard, B., and Lang, M.: Changes in Flood risk in Europe, edited by: Kundzewicz, Z. K., iAHS Special Publication 10, 199–211, 2012.

Giuntoli, I., Renard, B., Vidal, J.-P., and Bard, A.: Low flows in France and their relationship to large-scale climate indices, J. Hydrol., 482, 105–118, doi:10.1016/j.jhydrol.2012.12.038, 2013.

GRDC: French contribution to the Climate Sensitive Stations, available at: http://www.bafg.de/GRDC/EN/Home/homepage_node.html (last access: April 2017), 2015.

Habets, F., Boone, A., Champeaux, J. L., Etchevers, P., Franchistéguy, L., Leblois, E., Ledoux, E., Moigne, P. L., Martin, E., Morel, S., Noilhan, J., Segui, P. Q., Rousset-Regimbeau, F., and Viennot, P.: The SAFRAN-ISBA-MODCOU hydrometeorological model applied over France, J. Geophys. Res., 113, D06113, doi:10.1029/2007JD008548, 2008.

Hess, H.: Assimilation of screen-level observations by variational soil moisture analysis, Meteorol. Atmos. Phys., 77, 145–154, 2001.

Houser, P., Shuttleworth, W., Famiglietti, J., Gupta, H., Syed, K., and Goodrich, D.: Assessment of a multi-dimensional satellite rainfall error model for ensemble generation of satellite rainfall data, Water Resour. Res., 34, 3405–3420, 1998.

Jarlan, L., Balsamo, G., Lafont, S., Beljaars, A., Calvet, J.-C., and Mougin, E.: Analysis of leaf area index in the ECMWF land surface model and impact of latent heat on carbon fluxes: application to West Africa, J. Geophys. Res., 113, D24117, doi:10.1029/2007JD009370, 2008.

Jazwinski, A. H.: Stochastic Processes and Filtering Theory, Academic press, eBook, ISBN-13: 9780080960906, 150–158, 1970.

Kerr, Y. H., Waldteufel, P., Wigneron, J.-P., Martinuzzi, J.-M., Font, J., and Berger, M.: Soil moisture retrieval from space: the Soil Moisture and Ocean Salinity (SMOS) mission, IEEE T. Geosci. Remote, 39, 1729–1735, 2001.

Koster, R. and Suarez, M.: Modeling the land surface boundary in climate modls as a composite of independent vegetationstands, J. Geophys. Res., 97, 2697–2715, 1992.

Koster, R., Z.Guo, Yang, R., Dirmeyer, P., Mitchell, K., and Puma, M. J.: On the nature of soil moisture in land surface models, J. Climate, 22, 4322–4334, 2009.

Kumar, S. V., Reichle, R., Harrison, K., Peters-Lidard, C., Yatheendradas, S., and Santanello, J. A.: A comparison of methods for a priori bias correction in soil moisture data assimilation, Water Resour. Res., 48, W03515, doi:10.1029/2010WR010261, 2012.

Lafont, S., Zhao, Y., Calvet, J.-C., Peylin, P., Ciais, P., Maignan, F., and Weiss, M.: Modelling LAI, surface water and carbon fluxes at high-resolution over France: comparison of ISBA-A-gs and ORCHIDEE, Biogeosciences, 9, 439–456, doi:10.5194/bg-9-439-2012, 2012.

Le Moigne, P.: Description de l'analyse des champs de surface sur la France par le système SAFRAN, Technical report, Meteo-France/CNRM, 2002.

Ledoux, E., Girard, G., Marsily, G. D., and Deschenes, J.: Spatially distributed modeling: Conceptual approach, coupling surface water and ground water, in: Unsaturated Flow Hydrologic Modeling: Theory and Practice, NATO, ASI Series C, edited by: Morel-Seytoux, H., vol. 275, 435–454, 1989.

Maggioni, V., Anagnostou, E. N., and Reichle, R. H.: The impact of model and rainfall forcing errors on characterizing soil moisture uncertainty in land surface modeling, Hydrol. Earth Syst. Sci., 16, 3499–3515, doi:10.5194/hess-16-3499-2012, 2012.

Mahfouf, J.: Advances in model physics and their relevance to satellite data assimilation, Proceedings of the ECMWF seminar on the use of satellite observations in NWP, available at: http://www.ecmwf.int/sites/default/files/elibrary/, (last access: April 2017), 2014.

Mahfouf, J.-F.: Assimilation of satellite-derived soil moisture from ASCAT in a limited-area NWP model, Q. J. Roy. Meteor. Soc., 136, 784–798, doi:10.1002/qj.602, 2010.

Mahfouf, J.-F. and Noilhan, J.: Inclusion of gravitational drainage in a land surface scheme based on the force-restore method, J. Appl. Meteorol., 35, 987–992, 1996.

Mahfouf, J.-F., Bergaoui, K., Draper, C., Bouyssel, C., Taillefer, F., and Taseva, L.: A comparison of two off-line soil analysis schemes for assimilation of screen-level observations, J. Geophys. Res, 114, D08105, doi:10.1029/2008JD011077, 2009.

Meteo-France: SAFRAN atmospheric analysis, available at: http://mistrals.sedoo.fr/HyMeX/ (last access: April 2017), 2015.

Moradkhani, H., Hsu, K.-L., Gupta, H., and Sorooshian, S.: Uncertainty assessment of hydrologic model states and parameters: Sequential data assimilation using the particle filter, Water Resour. Res., 41, W05012, doi:10.1029/2004WR003604, 2005.

Moradkhani, H., DeChant, C. M., and Sorooshian, S.: Evolution of ensemble data assimilation for uncertainty quantification using the Particle Filter-Markov Chain Monte Carlo method, Water Resour. Res., 48, W2520, doi:10.1029/2012WR012144, 2012.

Moriasi, D., Arnold, J., Van Liew, M., Bingner, R., Harmel, R., and Veith, T.: Model evaluation guidelines for systematic quantification of accuracy in watershed simulations, American Society of Agricultural and Biological Engineers, 50, 885–900, 2007.

Muñoz Sabater, J., Jarlan, L., Calvet, J.-C., and Boyssel, F.: From Near-Surface to Root-Zone Soil Moisture Using Different Assimilation Techniques, J. Hydrometeorol., 8, 194–206, doi:10.1175/JHM571.1, 2007.

Nash, J. and Sutcliffe, J.: River flow forecasting through conceptual models, Part I – A discussion of principles, J. Hydrol., 10, 282–290, 1970.

Noilhan, J. and Mahfouf, J.-F.: The ISBA land surface parameterisation scheme, Global Planet. Change, 13, 145–159, 1996.

Quitana-Ségui, P., Moigne, P. L., Durand, P., Martin, E., Baillon, F. H. M., Canellas, C., and Franchistéguy, L.: Analysis of near-surface atmospheric variables: Validation of SAFRAN analysis over France, J. Appl. Meteorol. Clim., 47, 92–107, 2008.

Reichle, R. and Koster, R.: Global assimilation of satellite surface soil moisture retrievals into the NASA Catchment Land Model, Geophys. Res. Lett., 32, L02404, doi:10.1029/2004GL021700, 2005.

Reichle, R., Walker, J., Koster, R., and Houser, P.: Extended vs Ensemble Kalman Filtering for Land Data Assimilation, J. Hydrometeorol., 3, 728–740, 2002.

Reichle, R., Koster, R., Dong, J., and Berg, A.: Global Soil Moisture from Satellite Observations, Land Surface Models, and Ground Data: Implications for Data Assimilation, J. Hydrometeorol., 5, 430–442, 2004.

Reichle, R., Crow, W., and Keppenne, C.: An adaptive ensemble Kalman filter for soil moisture data assimilation, Water Resour. Res, 44, WO3243, doi:10.1029/2007WR006357, 2008.

Rüdiger, C., Albergel, C., Mahfouf, J.-F., Calvet, J.-C., and Walker, J.: Evaluation of the observation operator Jecobian for leaf area index data assimilation with an extended Kalman filter, J. Geophys. Res., 115, D09111, doi:10.1029/2009JD012912, 2010.

Scipal, K., Naeimi, V., and Hasenauer, S.: Definition of Quality Flags, ASCAT Soil Moisture Report Series, 7, 30 pp., available at: https://publik.tuwien.ac.at/files/PubDat_219473.pdf (last access: April 2017), 2005.

Scipal, K., Drusch, M., and Wagner, W.: Assimilation of a ERS scatterometer derived soil moisture index in the ECMWF numerical weather prediction system, Adv. Water. Resour, 31, 1101–1112, doi:10.1016/j.advwatres.2008.04.013, 2008.

Scott, D.: Multivariate Density Estimation: Theory, Practice, and Visualization, John Wiley & Sons, New York, Chicester, 1992.

Szczypta, C., Calvet, J.-C., Albergel, C., Balsamo, G., Boussetta, S., Carrer, D., Lafont, S., and Meurey, C.: Verification of the new ECMWF ERA-Interim reanalysis over France, Hydrol. Earth Syst. Sci., 15, 647–666, doi:10.5194/hess-15-647-2011, 2011.

Thirel, G., Martin, E., Mahfouf, J.-F., Massart, S., Ricci, S., and Habets, F.: A past discharges assimilation system for ensemble streamflow forecasts over France – Part 1: Description and validation of the assimilation system, Hydrol. Earth Syst. Sci., 14, 1623–1637, doi:10.5194/hess-14-1623-2010, 2010.

Vidal, J.-P., Martin, E., Franchistéguy, L., Baillon, M., and Soubeyroux, J.-M.: A 50-year high-resolution atmospheric analysis over France with the Safran system, Int. J. Climatol, 30, 1627–1644, doi:10.1002/joc.2003, 2010.

Vreugdenhill, M., Dorigo, W. A., Wagner, W., de Jeu, R. A. M., Hahn, S. M., and van Marle, J. E.: Analyzing the vegetation parameterization in the TU-Wien ASCAT soil moisture retrieval, IEEE T. Geosci. Remote, 54, 3513–3531, doi:10.1109/TGRS.2016.2519842, 2016.

Wagner, W., Lemoine, G., and Rott, H.: A method for estimating soil moisture from ERS scatterometer and soil data, Remote Sens. Environ., 70, 191–207, 1999.

Wagner, W., Blöschl, G., Pampaloni, P., Calvet, J.-C., Bizzarri, B., Wigneron, J.-P., and Kerr, Y.: Operational Readiness of Microwave Remote Sensing of Soil Moisture for Hydrologic Applications, Nordic Hydrol., 38, 1–20, doi:10.2166/nh.2007.029, 2007.

Walker, J. and Houser, P.: Hydrologic data assimilation, in: Advances in Water Science Methodologies, edited by: Aswathanarayana, U., A.A. Balkema, the Netherlands, p. 230, 2005.

Zhou, Y., McLaughlin, D., and Entekhabi, D.: Assessing the Performance of the Ensemble Kalman Filter for Land Surface Data Assimilation, Mon. Weather Rev., 134, 2128–2142, 2006.